INTERNATIONAL JOURNAL FOR NUMERICAL AND ANALYTICAL METHODS IN GEOMECHANICS, VOL. 21, 665–686 (1997)

MICROSTRUCTURE AND VOLUME CHANGE BEHAVIOUR OF SOFT CLAYS: A BOUNDARY ELEMENT SIMULATION

M. CERROLAZA*,[1] AND P. DELAGE†,‡,[2]

[1] *Instituto de Materiales y Modelos Estructurales, Facultad de Ingenieria, Universidad Central de Venezuela, P.O. Box 50.361, Caracas 1050-A, Venezuela*
[2] *Centre d'Enseignement et Recherche en Mécanique des Sols (CERMES), Ecole Nationale des Ponts et Chaussées, 93167 Noisy Le Grand Cedex, France*

SUMMARY

The relationship between the microstructure and the volume change behaviour of fine-grained soft soils is analysed by using a model derived from the experimental observation of the microstructure of soft clays, and the Boundary Element Method (BEM). The soil is modelled as a bidimensional porous matrix containing circular pores. The matrix is linear elastic and obeys a Tresca failure criterion, and the pore size distribution follows a Gaussian normal law. The pores are randomly located, with a minimum distance between them. Volume decrease during compression is due to the collapse of the pores. The collapse of a pore is activated once the stress state at the pore boundary calculated by the BEM is reaching the Tresca failure criterion, thus leading to a non-linear analysis process. An isotropic incremental loading test as well as a loading–unloading test are presented and discussed, showing that the model is able to reproduce properly the experimental volume change behaviour of soft clays and other porous geomaterials like chalk. Numerical results show that a macroscopic hardening elastoplastic behaviour could be obtained from a model elaborated from microstructure observation. © 1997 by John Wiley & Sons, Ltd.

Int. J. Numer. Anal. Meth. Geomech., Vol. 21, 665–686 (1997)
(No. of Figures: 17 No. of Tables: 0 No. of Refs: 41)

1. INTRODUCTION

The microstructure of soils is often represented as an assembly of grains with punctual contacts. This representation is valid for sands, but approximate for fine-grained soils, which are made of clay platelets, generally aggregated together. Another big difference is related to the physico-chemical bonds acting between the clay particles and the water molecules in fine-grained soils, which do not exist in granular soils. These clay–water interactions are quantified at a macroscopic level by the Atterberg limits. However, it is current practice in soil mechanics to consider fine-grained soils as granular media, and to interpret their mechanical behavior in terms of

*Professor
†Senior Researcher
‡Correspondence to: P. Delage, CERMES, ENCP, 93167 Noisy Le Grand Cedex, France

Contract grant sponsor: CERMES; contract grant sponsor: Ecole Nationale des Ponts et Chaussées; contract grant sponsor: Consejo de Desarollo Científico y Humanístico (Caracas)

CCC 0363–9061/97/100665–22$17.50

Received 20 June 1996
Revised 1 February 1997

relative movements and spatial reorganization of grains. For sands, various micromechanical analysis have been developed for understanding the macroscopic behavior. Fewer attempts have been made in fine-grained soils.

The investigation of the microstructure of fine-grained soils has developed in the last 30 years in the case of natural soft clays, which exhibit a large compressibility and a poor mechanical resistance, and can be a problem when building earth structures or foundations on them. Early work was made using scanning electron microscope. Mercury intrusion pore size distribution measurements were also used. 'Pore collapse' mechanisms were identified during compression, suggesting that soft clays could also be considered as porous solids, with a volume change behaviour depending on the pore size distribution and the mechanical properties of the solid matrix.

The mechanism of pore collapse was analytically studied in a very simple two-dimensional model made of a matrix containing a unique circular pore.[1] Taking a linear isotropic elastic matrix also obeying a Tresca failure criterion, Morlier analytically predicted the pore collapse and determined the failure criterion of the porous solid. In this work, a similar model of porous medium containing more pores of different sizes is considered in order to extend the approach to the analysis of the volume change behavior of soils and other porous media. A specific numerical algorithm based on the Boundary Element Method (BEM) is developed in order to tackle this problem, and a macroscopic model for fine grained soils based on mechanisms occurring at a microscopic level is proposed.

2. THE MICROSTRUCTURE OF SOFT SOILS

Models of the microstructure of fine-grained soils have been considered very early on by geotechnical engineers in order to help in understanding some aspects of their behaviour, such as sensitivity.[2] In all early conceptual models, the elementary particle type considered was the single clay platelet. This is the case of Lambe's model[3] for compacted soils, which was based on the double-layer theory. Since Lambe developed his theory, there have been significant improvements in the techniques of observing microstructures, leading to a more and more complete description of the microstructure of fine grained soils in relation to their mechanical behaviour. This evolution is described in various papers concerning sensitive clays,[4] various natural soils,[5] and in special conferences dedicated to soil microstructure.[6,7] Recent conferences on this subject provide a complete description of many related problems, including the latest technical developments, physicochemical phenomena affecting the formation and evolution of microstructures in relation with environmental conditions, and applications related to environmental engineering.[8] As compared to earlier simple conceptual fabric models, it has been shown that the basic element of the microstructure of natural soils is not the single clay platelet, but domains constituted of various platelets aggregated together.[9] Indirect evidence of the existence of aggregates was also obtained from hydraulic conductivity tests by Olsen.[10] In some cases, these aggregates can be resistant to some macroscopic mechanical actions. For a medium-sensitive Canadian clay, Delage and Lefebvre[11] showed that aggregates were still existing in the remoulded state.

An extensive study of the pore-size distributions of various sensitive clays of Eastern Canada[12] was performed using mercury intrusion porosimetry. Mercury porosimetry is based on the principle that a non-wetting fluid, such as mercury, does not enter a porous medium unless a pressure is applied. Comparing pores to circular capillaries, the pressure P is related to an

entrance pore radius r by Laplace's law

$$P = \frac{2\sigma \cos \theta}{r} \tag{1}$$

where σ is the surface tension of the intruding liquid and θ the contact angle (for mercury, $\theta = 141^\circ$ and $\sigma = 0{\cdot}484$ N/m). As the pressure P is increased, pores of smaller and smaller radii are intruded. The results are plotted in a cumulative curve, giving the pore size distribution of the porous medium.

Figure 1 (Reference 13) shows the pore size distribution (PSD) curve of a medium sensitive clay of eastern Canada (St. Marcel clay). The PSD curve has a regular unimodal shape, with a well-sorted pore population defined by the inflection point, at a radius of 0·18 μm. The pore size distribution is further precised by the derivative curve, which shows that the distribution is approximately Gaussian.

Figure 2 shows scanning electron photomicrographs of the St. Marcel clay. An elementary 2 μm diameter aggregate is shown in Figure 2(c). Smaller magnifications (Figures 2(a) and 2(b)) show the overall regular aspect of the aggregate microstructure. An inter-aggregate porous network is surrounding the aggregates. The average dimension of the inter-aggregate pores is close to 0·5 μm. The dimensions of the inter-aggregate pores are slightly underestimated by mercury intrusion, which defined an average 0.36 μm diameter. These is a well-known limitation of mercury porosimetry, which is only able to ensure an entrance pore value in the case of ink-bottle pores.

The compression curve of the St. Marcel clay is shown in Figure 3. The shape of the curve is typical of structured clays. Very small strains are observed at low stresses, where the initial structure is remaining intact. Above 50 kPa, a sudden volume decrease occurs. The evolution of the microstructure at this stage was studied in detail by Delage and Lefebvre,[11] who showed that the sudden volume decrease corresponded to the collapse of pores, starting with the larger ones, and affecting progressively smaller and smaller pores. This mechanism was also observed on various other sensitive clays by comparing oedometric compression curves and PSD curves.[12,13] The pore collapse mechanism has also been observed on other porous geomaterials. In oil

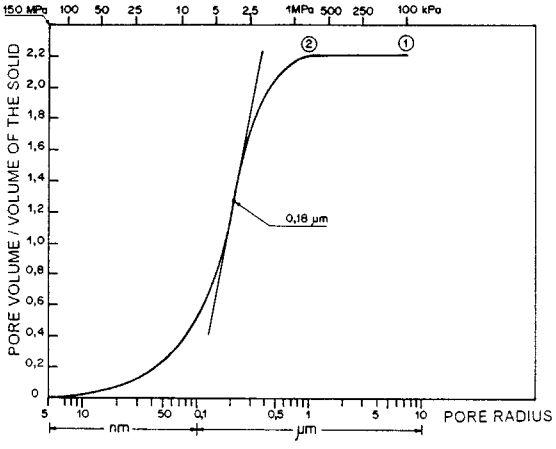

Figure 1. Pore size distribution (PSD) of a medium-sensitive clay of Eastern Canada (St. Marcel clay)

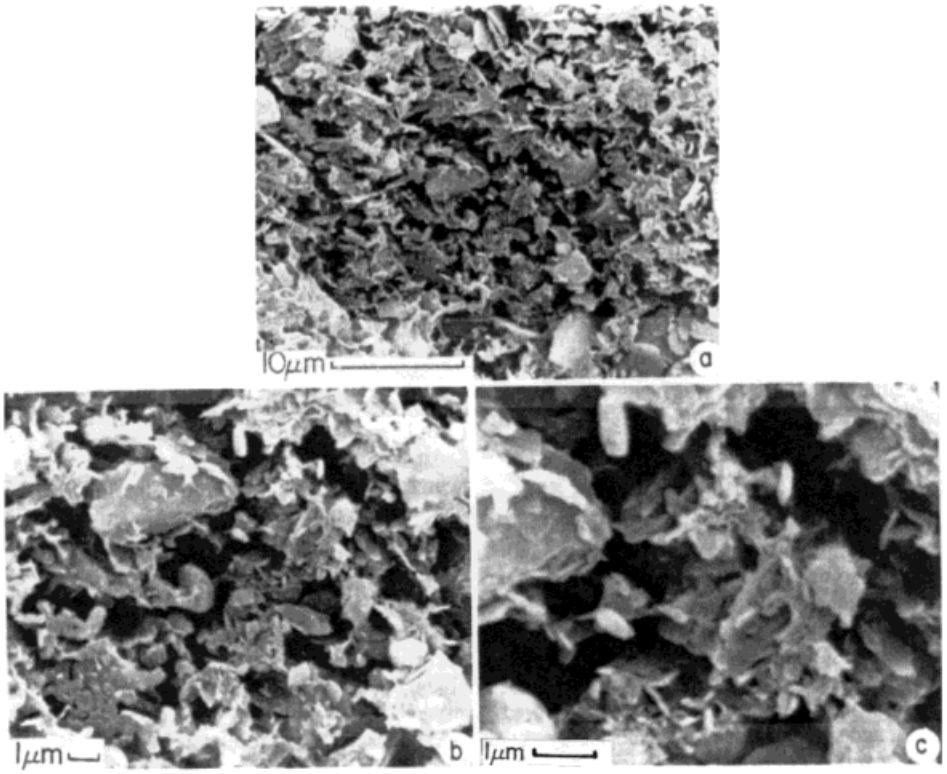

Figure 2. Electron photomicrographs of the clay

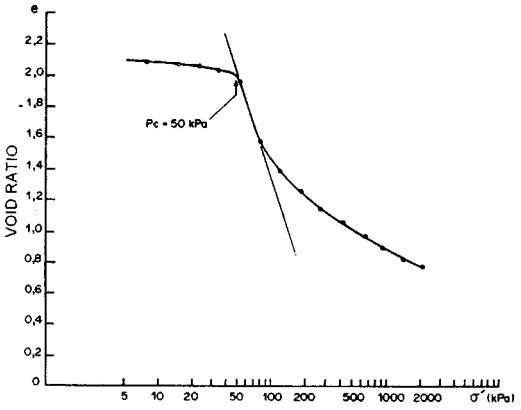

Figure 3. Compression curve for the St. Marcel clay

engineering, it occurs in high porosity chalk reservoirs (porosities higher than 50 per cent). It is quite a big concern because of the subsidence induced during oil exploitation.[14–16]

More generally, various similarities between weak rocks and structural soils have been evidenced by Leroueil and Vaughan.[17] Another typical feature of their common brittle behaviour

is observed in triaxial shear tests at low confining stresses. The stress–strain curves present a fairly steep initial linear segment, and failure occurs at small strains and corresponds to a sharp peak. Before the peak, the structure remains apparently intact, with a fairly reversible response to cyclic loading. Failure is abrupt and coincides with the formation of shear surfaces.

In order to study the elastic domain of porous media, Morlier[1] considered a simple model of a porous medium made of a linear isotropic elastic matrix containing a unique spherical pore (Figure 4(a)). He used the results of Goodier,[18] who determined the stress concentration around the spherical pore of Figure 4(a) by giving the principal local stresses s_i applied by a $(\sigma_1, 0, 0)$ stress at the points A, B and C:

Point A:
$$s_1 = 0, \qquad s_2 = s_3 = -\frac{3 + 15v}{14 - 10v}\sigma_1. \tag{2}$$

on BCB′C′:
$$s_1 = \frac{27 - 15v}{14 - 10v}\sigma_1, \quad s_2 \text{ or } s_3 = 0, \quad s_3 \text{ or } s_2 = -\frac{3 - 15v}{14 - 10v}\sigma_1 \tag{3}$$

v being the Poisson ratio of the elastic material. By considering a Tresca failure criterion for the matrix, Morlier showed that the failure of the model was caused by the pore collapse, which occurred when the Tresca criterion was reached at the border of the pore. By using expressions (2) and (3), he showed that the elastic domain of the simplified model was closed (see Figure 4(b)). This approach demonstrated that it was possible to predict the mechanical resistance of a porous medium knowing the mechanical properties of the matrix and the dimension of the pores.

In the following, based on the observation of the microstructure of sensitive clays, the previous approach will be extended to the analysis of the volume change behaviour of soft clays and other porous media. A two-dimensional model made of a linear isotropic elastic matrix containing circular pores of various diameters and obeying a Tresca failure criterion will be considered. Due to the larger complexity of the problem, calculations of the stresses at the border of the pores will be made by using the boundary element method.

This first model will not consider the role of water, but only the response of the solid skeleton of the soil, i.e. the drained response of the soil. The complete problem including the effects of water circulation and the pore pressure dissipation could be considered later in a more complete model also including interconnections between pores, and flow of water within the porous network.

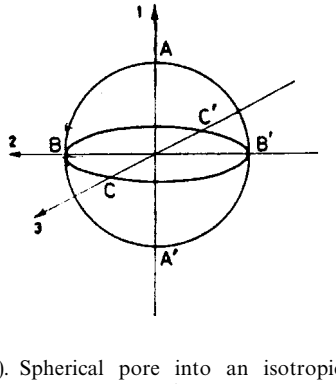

Figure 4(a). Spherical pore into an isotropic elastic matrix

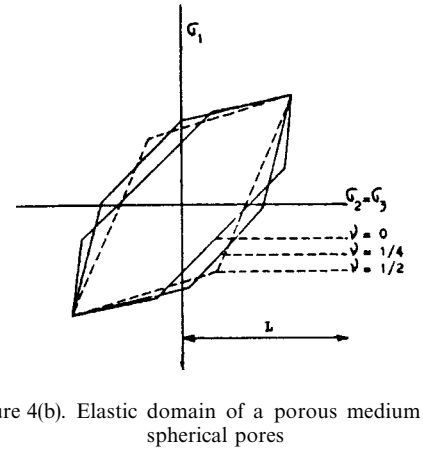

Figure 4(b). Elastic domain of a porous medium with spherical pores

3. NUMERICAL MODELLING OF THE SOIL MICROSTRUCTURE

Much effort with the BEM has been done recently in the area of geomechanics, both at macroscopic and microscopic scales. At the macroscopic level, the technical literature displays several works doing numerical simulation with boundary elements in soil mechanics and flow in porous media. Dominguez[19] presented a BEM direct formulation for evaluating the dynamic response of poroelastic bidimensional media, while Rajapakse and Senjuntichai[20] have presented an indirect formulation for the same topic. Ohkami *et al.*[21] worked with orthotropic geomaterials by applying BEM. The simulation of consolidation processes in elastic soils is discussed by Chiou and Chi,[22] who have analysed the Biot's consolidation in three-dimensional layered domains. Chopra and Dargush[23] also applied the BEM to the time domain analysis of consolidation process in an axisymmetric model. In the field of flow in unsaturated media, a great amount of scientific research has also been done. Martinez and McTigue[24] presented a BEM formulation for the analysis of a partially saturated medium using a hydraulic conductivity that varies with the capillary-pressure head.

At the microscopic scale, many authors have investigated multi-phase Navier–Stokes flow in disordered microporous media by using lattice-Boltzman models. Gunstensen and Rothman[25] presented the ideas to analyse a two-phase flow porous media. Soll *et al.*[26] analysed the multi-fluid flow in porous media, also using lattice-Boltzman methods, while Ginzsbourg and Adler[27] studied the boundary conditions in three-dimensional lattice-Boltzman models. These works, among other well-known works, show the interest of the scientific community in the study of the microstructure of soils. Other authors have presented and discussed model for soil-pore analysis based on pseudo-fractal sets (see Reference 28). Also Moran and Kirby [29] presented a soil-pore model based on random generation of bidimensional continua by using a set of linear porosity elements. These elements can represent the changes in porosity by a porosity value, which takes the value of zero in fully solid elements and the value of one in fully pored elements.

This section is concerned with a brief presentation of the BEM applied to internal problems as well as a description of the BEM model used to represent the soil microstructure. The approach is based on the integral equation formulation written in terms of the boundary displacements.

3.1. The boundary element method

A detailed formulation of the BEM can be found in the technical literature as, for instance, References 30–33 among others. This work uses the BEM direct formulation, based on the Somigliana's identity, which provides the unknown variable fields over the boundary. Likewise, a two-dimensional model is used, since the problem herein is well described by a plane strain model, and by considering an *interior problem*: a domain (soil microstructure) enclosed by a finite boundary.

Let R be an infinite, elastic, isotropic and homogeneous medium, limited by the boundary S, as shown in Figure 5. This boundary also is divided into two sub-boundaries called S_u and S_t (kinematic and static boundary).

Then the boundary conditions could be expressed as

$$u_i(Q) = \bar{u}_i(Q) \quad \text{in } S_u, \quad t_i(Q) = \bar{t}_i(Q) \quad \text{in } S_t \qquad (i = 1, 2)\ (Q \in S) \tag{4}$$

where $u_i(Q)$ and $t_i(Q)$ are the displacements and tractions fields over the boundary, and the bar – states for *known fields*. Following Somigliana's development,[30] the solution to the elastic

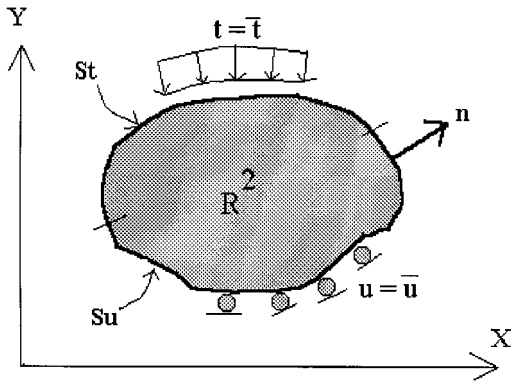

Figure 5. Boundary conditions in interior problems

problem can be obtained by the relation.

$$u_i(P) = \int_S [u_{ij}^*(P, Q)\, t_j(Q) - t_{ij}^*(P, Q) u_j(Q)]\, \mathrm{d}S(Q) + \int_\Omega u_{ij}^*(P, Q) F_j(Q)\, \mathrm{d}\Omega(Q)$$

$$(P \in \Omega), (Q \in S) \tag{5}$$

The above equation is a function of the displacement and stress fields over the boundary S and of the known gravitational forces $F_j(Q)$. The application of equation (5) requires the previous knowledge of the tensors $u_{ij}^*(P, Q)$ and $t_{ij}^*(P, Q)$, which represent the displacements and tractions acting at a point Q in the j direction due to unit forces acting at a point P in the i direction. These functions are due to Lord Kelvin (see Reference 34) and correspond to the singular solutions of the Navier equations. In the case of two dimensions (plane strain), they take the form

$$u_{ij}^*(P, Q) = \frac{1}{8\pi G(1 - \nu)} [(3 - 4\nu) \log(r^{-1}) \delta_{ij} + r_{,i} \cdot r_{,j}]$$

$$t_{ij}^*(P, Q) = -\frac{1}{4\pi(1 - \nu)} \frac{1}{r} \{[(1 - 2\nu)\delta_{ij} + 2r_{,i} \cdot r_{,j}] r_{,n} - (1 - 2\nu)(r_{,i} n_j - r_{,j} n_i)\} \tag{6}$$

r being the distance from load point P and field point Q and is expressed as

$$r = [r_i(P, Q) \cdot r_i(P, Q)]^{1/2} \tag{7}$$

where

$$r_i(P, Q) = r_i(Q) - r_i(P) \tag{8}$$

The derivatives $r_{,i}$ as well as the normal vector n_i to the body surface are taken with respect to the Q-co-ordinates, which means

$$r_{,i} = \frac{\partial r_i(P, Q)}{\partial x_i(Q)} = \frac{r_i(P, Q)}{r} \tag{9}$$

As the boundary problem is treated only as a function of the known variable fields at points on its S boundary, expression (5) should be modified in order to be able to handle the solution at

boundary points. This expression is also follows.

$$C_{ij}(P)u_j(P) = \int_S [u^*_{ij}(P, Q)t_j(Q) - t^*_{ij}(P, Q)u_j(Q)]\, \mathrm{d}S(Q) + \int_\Omega u^*_{ij}(P, Q)F_j(Q)\, \mathrm{d}\Omega(Q) \quad (P, Q \in \Omega) \quad (10)$$

The use of the last expression requires the previous evaluation of the $C_{ij}(P, Q)$ matrix, which terms depend only on the boundary geometry at the vicinity of points P where the unit load is applied. There exist some mathematical formulation[33] that allows the evaluation of the C_{ij} matrix as a function of the angle defined by the two normal vectors at the non-smooth point P, as follows:

$$C_{ij}(P) = \begin{bmatrix} 2\Delta\alpha(1-\nu) + \frac{1}{2}(\sin 2\alpha_1 - \sin 2\alpha_2) & \sin^2\alpha_1 - \sin^2\alpha_2 \\ \sin^2\alpha_1 - \sin^2\alpha_2 & 2\Delta\alpha(1-\nu) - \frac{1}{2}(\sin 2\alpha_1 - \sin 2\alpha_2) \end{bmatrix} \quad (11)$$

α_1 and α_2 being the angles of the normal vectors with the corresponding boundary elements and $\Delta\alpha$ the angle between these two elements. In the two-dimensional case this matrix is

$$C_{ij}(P) = \begin{cases} \delta_{ij} & \text{if } P \in \Omega \\ \frac{1}{2}\delta_{ij} & \textit{if } P \in S \text{ and } S \text{ is is smooth} \\ 0 & \text{if } P \notin Q, S \end{cases} \quad (12)$$

The unknown variable fields can be computed at points P inside the domain by using the Somigliana's equation (5). To evaluate the stress fields it is then necessary to obtain the $\varepsilon_{ij}(P)$ strain tensor by derivating equation (7), thus arriving at

$$\varepsilon_{ij}(P) = \int_S [u^*_{ijk}(P, Q)t_k(Q) - t^*_{ijk}(P, Q)u_k(Q)]\, \mathrm{d}S(Q) + \int_\Omega [u^*_{ijk}(P, Q)F_k(Q)\, \mathrm{d}\Omega(Q) \quad (13)$$

where the operators $u^*_{ijk}(P, Q)$ and t^*_{ijk}(P, Q) result from derivating the functions $u^*_{ij}(P, Q)$ and $t^*_{ij}(P, Q)$ with respect to the Cartesian co-ordinates at point P. Now, by introducing equation (13) into the stress–strain relation

$$t_{ij}(P) = 2G\left[\varepsilon_{ij}(P) + \delta_{ij}\frac{\nu}{1+\nu}\varepsilon_{kk}(P)\right] \quad (14)$$

The desired expression for the $t^*_{ij}(P, Q)$ at P is obtained as

$$t_{ij}(P) = \int_S [D^*_{ijk}(P, Q)t_k(Q) - S^*_{ijk}(P, Q)u_k(Q)]\, \mathrm{d}S(Q) + \int_\Omega [D^*_{ijk}(P, Q) - F_k(Q)\, \mathrm{d}\Omega(Q) \quad (15)$$

where the third-order tensors have the form[30]

$$D^*_{ijk}(P, Q) = \frac{1}{4\alpha\pi(1-\nu)}\frac{1}{r}\left[(1-2\upsilon)(\delta_{jk}r_{,i} + \delta_{ik}r_{,j} - \delta_{ij}r_{,k}) + \beta r_{,i}r_{,j}r_{,k}\right] \quad (16)$$

$$S^*_{ijk}(P, Q) = \frac{G}{2\alpha\pi(1-\nu)}\frac{1}{r}\{\beta r_{,n}[(1-2\upsilon)\delta_{ij}r_{,j} + \delta_{jk}r_{,i} - \gamma r_{,i}r_{,j}r_{,k}] + \beta\upsilon(n_i r_{,j}r_{,k} + n_j r_{,i}r_{,k}) + (1-2\upsilon)(\beta n_k r_{,i}r_{,j} + n_j\delta_{ik} + n_i\delta_{jk}) - (1-4\upsilon)n_k\delta_{ij}\} \quad (17)$$

with $\alpha = 1$, $\beta = 2$ and $\gamma = 4$ for plane strain.

3.2. Discretization of the geometry and variable fields over the boundary

Two-noded linear boundary elements are chosen for the boundary discretization because of its simplicity and clarity. However, boundary elements of higher order with more than two nodes can be used with no further difficulties.[35,36] Once the boundary is discretized into N_e elements

$$S = \sum_{k=1}^{N_e} S_k \tag{18}$$

the displacements and stresses fields as well as the geometry over the element S_k are represented as follows:

$$\begin{aligned} u_i(Q) &= \sum_{j=1}^{N_k} F^j(Q) u_i^j \quad (\text{in } S_t,\ Q \in S_k) \\ t_i(Q) &= \sum_{j=1}^{N_k} F^j(Q) t_i^j \quad (\text{in } S_u,\ Q \in S_k) \\ x_i(Q) &= \sum_{j=1}^{N_k} F^j(Q) x_i^j \quad (\text{in } S,\ Q \in S_k) \end{aligned} \tag{19}$$

where N_k is the number of interpolation functions used to represent the variables and the boundary geometry. In our case, $N_k = 2$ since each element is defined by only two nodes. The $F^j(Q)$ functions can be expressed in the isoparametric space $\xi = [-1, 1]$ in order to carry out the numerical integration of the stiffness coefficients. Thus, equations (19) can be rewritten as

$$u_i(Q) = \sum_{j=1}^{2} F^j(\xi) u_i^j, \qquad t_i(Q) = \sum_{j=1}^{2} F^j(\xi) t_i^j, \qquad x_i(Q) = \sum_{j=1}^{2} F^j(\xi) x_i^j \tag{20}$$

On the other hand, it will be necessary to have an expression to determine the normal outward vector as well as another expression to evaluate the Jacobian. By derivating equation (20) with respect to ξ, we obtain the boundary tangent vector

$$s_i(\xi) = \frac{\mathrm{d}x_i(\xi)}{\mathrm{d}\xi} = \sum_{j=1}^{2} \frac{\mathrm{d}F^j(\xi)}{\mathrm{d}\xi} x_i^j \tag{21}$$

and therefore the Jacobian is

$$J(\xi) = \| s_i(\xi) \| = \left[\sum_{j=1}^{2} \left(\frac{\mathrm{d}F^j(\xi)}{\mathrm{d}\xi} x_i^j \right)^2 \right]^{1/2} \tag{22}$$

Thus, the components of the outward normal can be calculated as

$$n_1(\xi) = \frac{s_2(\xi)}{J(\xi)}, \qquad n_2(\xi) = -\frac{s_1(\xi)}{J(\xi)} \tag{23}$$

Now, by substituting equations (22) and (23) into the Somigliana identity and neglecting the effect of body forces, one obtains

$$C_{ij}(P) u_j(P) = \sum_{k=1}^{N_e} \sum_{l=1}^{2} \left[U_{ij}^l(P, Q) t_j(Q) - T_{ij}^l(P, Q) u_j(Q) \right] \mathrm{d}S(Q) \tag{24}$$

with

$$T_{ij}^{l}(P, Q) = \int_{S_k} t_{ij}^{*}(P, Q) F^{l}(Q)\, \mathrm{d}S(Q)$$
$$U_{ij}^{l}(P, Q) = \int_{S_k} u_{ij}^{*}(P, Q) F^{l}(Q)\, \mathrm{d}S(Q) \tag{25}$$

When the integral expression (24) is written for the N nodes of the boundary (points P^k, $k = 1$ to N) the following matrix expression is obtained:

$$A_{ij} u_j - B_{ij} t_j = 0 \tag{26}$$

where

$$A_{ij}^{kl}(P^k) = C_{ij}(P^k) + \int_{S_k} t_{ij}^{*}(P^k, Q) F^{l}(Q)\, \mathrm{d}S(Q) \tag{27}$$

and

$$B_{ij}^{kl}(P^k) = \int_{S_k} u_{ij}^{*}(P^k, Q) F^{l}(Q)\, \mathrm{d}S(Q) \tag{28}$$

The imposition of the boundary conditions (4) to expression (26) leads to a system of equations of order $2N$, which is written as follows:

$$K_{ij} u_j = P_i \tag{29}$$

u_i being the vector containing all the unknowns (displacements and tractions at the boundary) and K_{ij} the stiffness matrix. P_i is the vector containing the known quantities at the boundary.

3.3. A simplified 2D model: analysis of a randomly generated microstructure

The bidimensional model proposed in this work is derived from PSD measurements on soft clays described in Section 2. It is based on the random generation of circular pores into a bidimensional continuous medium simulating the soil skeleton. The distribution of the radii of the pores is Gaussian normal, as shown in Figure 6.

The algorithm randomly generates the required number of pores until the previously specified void ratio $e = V_v/V_s$ is reached (V_v being the void volume and V_s the volume of solids). Together with the desired void ratio e, the following Gaussian-distribution parameters have to be supplied: Φ_{min} the minimum radius of pores; Φ_{max} the maximum radius of pores; Φ_{med} the mean radius of pores; and S_{dev} standard deviation of Gaussian distribution.

As shown in Figure 6(a), the bidimensional model displays two zones: the *internal* zone ($L_x * L_y$ dimensions) which contains the pores generated, while the *extended* zone of larger dimensions is necessary to apply properly the external pressures to the boundary element model. Numerical experiments have shown that these extensions in both directions are enough for practical purposes. For generating the soil microstructure, the algorithm also requires the definition of d_m the minimum distance between two pores (see Figure 7), E the Young's modulus of the matrix and v the Poisson's ratio of the matrix.

The Cartesian co-ordinates of the central point P_i of each pore are, therefore, randomly generated inside the central zone $L_x * L_y$, as shown in Figure 7.

Once the algorithm has verified that the pore being generated is valid, i.e. the pore fits into the central zone and it does not intersect any other previously generated pore, the pore is stored. This process is repeated until the desired void ratio is reached.

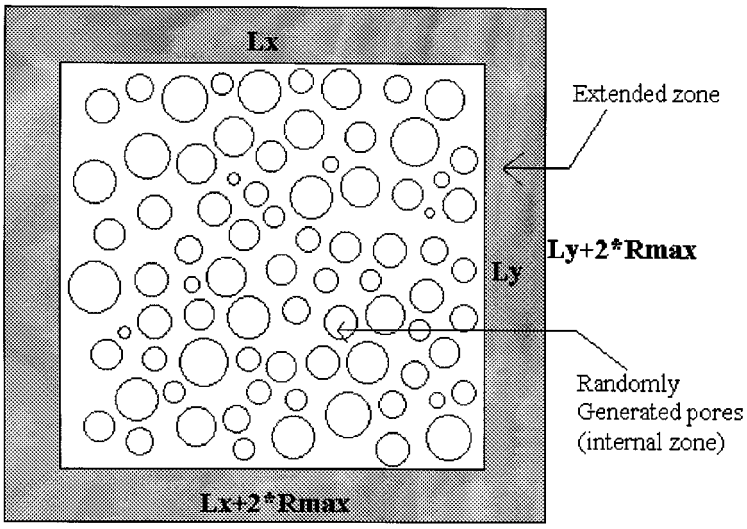

Figure 6(a). Model of soil microstructure: R_{max} = maximum diameter of pores

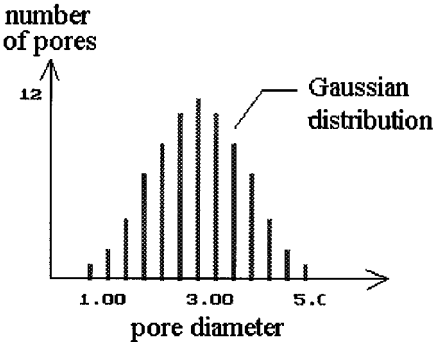

Figure 6(b). Typical Gaussian distribution of pores

When the generation of the model is completed, the pores are discretized in the same way as the exterior boundary of the extended zone by using straight boundary elements, as illustrated in Figure 8. Six boundary elements were used to discretize the boundary of each pore. The boundary of the extended zone is also discretized by using six boundary elements per side, in order to apply the external pressures. Some sensitivity tests have shown that six boundary elements are accurate enough to represent properly the pore. The algorithm can create a refined model by using, for instance, eight, 12 or 16 boundary elements per pore, but the CPU time will substantially increase and it is not necessary from an engineering and practical point of view. The boundary elements used in this work are two-noded and linear interpolation of the variable fields are used. Of course, a refined interpolation could be employed, say higher-order elements of three or more nodal points.[31,36] However, as pointed out before, our sensitivity analyses have shown that no relevant improvement is obtained by using higher interpolations.

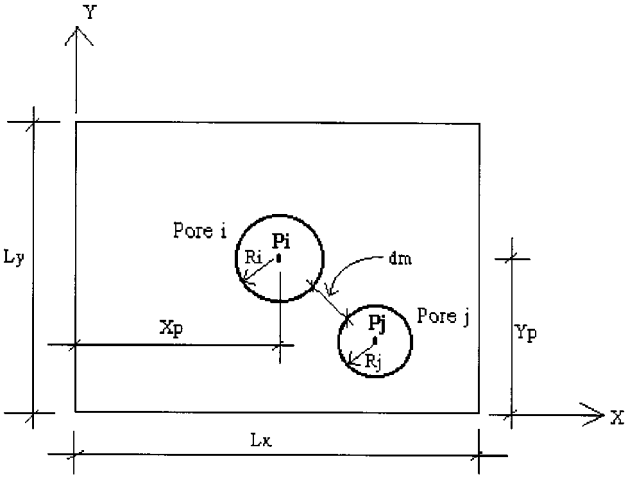

Figure 7. Further geometric definitions: minimum distance between two adjacent pores

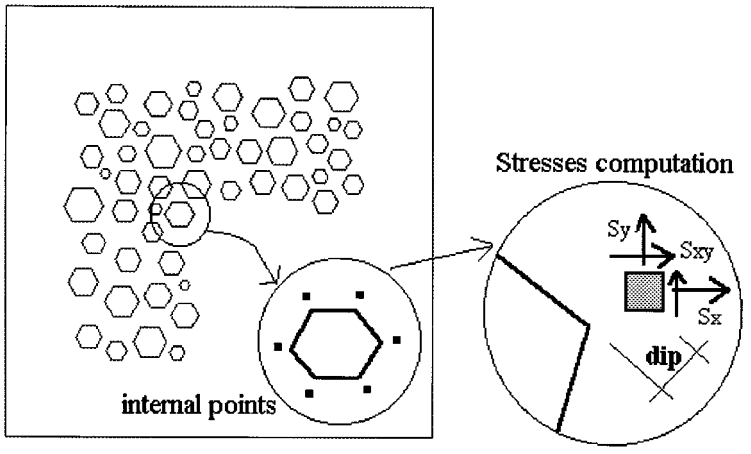

Figure 8. Boundary element discretization and internal points to compute stresses

The algorithm also generates the required internal points where the stress tensor must be computed, according to expression (15). These internal points are generated very close to the pore boundary, displaying a maximum distance called 'Dip', which is determined using the following criterion: if $d_m < 0{\cdot}1R_i$ then Dip $= d_m/2$ else Dip $= 0{\cdot}05R_i$, 'd_m' being the minimum distance allowed between two adjacent pores (see Figure 8) and R_i the radius of the pore. Another question that deserves further comments is the numerical integration approach. As noted in equations (16) and (17), the quasi-singular kernels appearing into the boundary integrals are strongly dependent on the distance 'Dip' (r in the cited equations) from the internal point to the boundary element under consideration. Much effort has been done in trying to integrate accurately such kernels, but

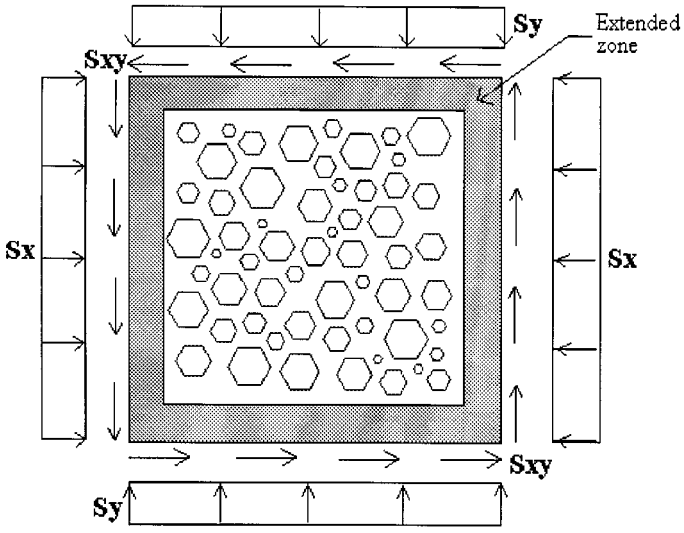

Figure 9. External pressures applied at the extended zone of the microstructure model

their discussion is beyond the scope of this work. The reader interested in the formulae details of such techniques should refer to References 37–40.

Once the boundary discretization is done, the user is requested to provide the external pressures, which are to be applied on the model. It is possible to carry out non-isotropic simulations by applying different pressures at the external boundary, as displayed in Figure 9. As illustrated, both normal and shear stresses can be defined in the model, thus allowing the possibility to carry out many different numerical simulations.

3.4. The numerical process as a whole

The above-described dimensional boundary element model is then processed according to the BEM formulation already discussed. An increasing load is applied to the model, and the stresses are calculated after each load increment at the 6 internal points (see Figure 8) of the pore boundaries, according to the linear elastic properties of the solid matrix. If the Tresca criterion is reached in a point at a pore boundary, ($\sigma_{max} = |\sigma_1 - \sigma_3|$ where σ_1 and σ_3 are the principal stresses at the point), the pore is collapsed and its volume reduced to zero. The steps of the incremental procedure are summarized below:

Step	Action
1	Set up and initialization of algorithm parameters. Set up of the initial external pressures.
2	Generate the system of equations (29) by considering the external loading.
3	Solve the system (29) thus obtaining the displacements at every boundary point in the model.
4	Compute the strain and stress fields at every internal point by using equations (13) and (15).

5 For each pore check if the highest elastic stress at the boundary has exceeded the limit stress, by comparing with the Tresca criterion of the matrix: $\sigma_{max} = |\sigma_1 - \sigma_3|$, where σ_{max} is the elastic limit stress allowed in the soil. Also, mark each pore that is collapsed, i.e. the cracked pores.

6 Delete all collapsed pores from the model and renumber the whole model. As expected, the void ratio e decreases since the void volume V_v decreases as pores are deleted.

7 Increase the applied external pressures with a previously defined increment.

8 Go to step 2. The process ends when no more pores remain.

The described process is a non-linear analysis process, since the model geometry changes at every iteration. Thus, it is necessary to select the load increment carefully in order to follow smoothly the evolution of the model behaviour.

4. VALIDATION AND DISCUSSION OF THE NUMERICAL RESULTS

The validation of the previous numerical simulation is presented and discussed through two simulations: an incremental loading process, and a loading–unloading process.

4.1. Continuously incremental loading

The randomly generated circular pores of the model are presented in Figure 10. The model is defined by the following parameters: number of pores = 58; $\phi_{MIN} = 0{\cdot}1$ μm; $\phi_{MAX} = 0{\cdot}46$ μm; $\phi_{MED} = 0{\cdot}18$ μm; $d_m = 0{\cdot}1$ μm; $S_{dev} = 0{\cdot}2$ μm; $e = V_v/V_s = 1{\cdot}40$.

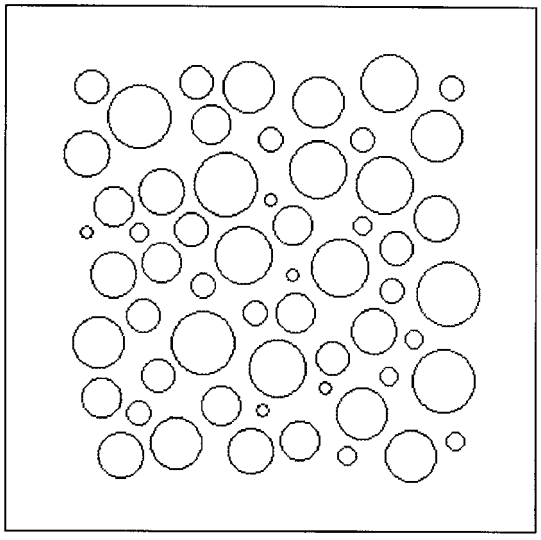

Figure 10. Randomly generated pores for the case example

The number of pores (58) has been chosen after running various sensitivity tests aimed at keeping within reasonable limits the CPU time (150 min) on a 486DX personal computer. More pores could be considered when using more powerful workstations.

Figure 11 displays the BEM model corresponding to Figure 10, which has been discretized by using six boundary elements per pore.

The choice of the Young modulus of the solid matrix is not an evident and easy task. In fact, it may be derived from a compression test performed on a soil at a high stress, where most of the pores have been collapsed, and where the compressibility of the clay matrix is involved. A value of 50 MPa has been considered as being realistic. Of course, more information on this value can be obtained by running a specific experimental program. A standard value of 0·3 has been taken for Poisson's ratio. This also could be experimentally confirmed by running tests with measurements of lateral stresses.

The initial applied pressure is 100 kPa. The test simulated an isotropic compression test where the pressure increased by 20 kPa increments up to a stress of 280 kPa. Once the simulation process is completed, the program creates a file containing all relevant information such as number of iterations of the non-linear analysis, external pressures and void ratio at each step and value of the highest stress of each pore on its boundary.

Figure 12 shows the compression curve calculated with the numerical model proposed herein, giving the void ratio as a function of the logarithm of the total isotropic stress, like for standard oedometric curves. The shape of the curve is in a satisfactory agreement with that of structured soft soils, such as the one presented in Figure 3: a negligible strain is observed below a given stress value, followed by an increasing slope with a maximum between 140 and 160 kPa. Finally, the slope decreases as the stress increases. As for natural soils, this trend can be interpreted in terms of pore collapse. Below 100 kPa, all pores are able to support the load, leaving the microstructure intact. The pore collapse starts above 100 kPa, and a large pore volume is destroyed between 140

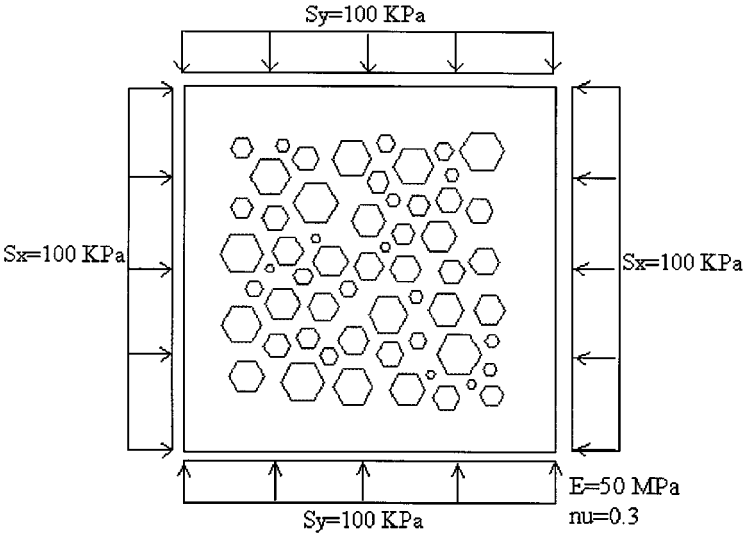

Figure 11. Boundary element model for the case example

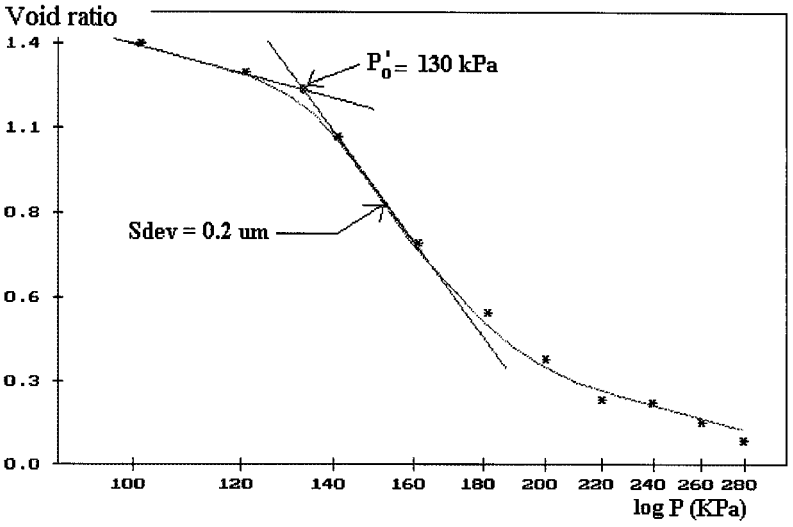

Figure 12. Evolution of the void ratio VS $\log(\sigma)$ in example case. Gaussian distribution. $S_{dev} = 0{\cdot}2$ μm

and 160 kPa, defining a compression index C_c ($C_c = \Delta e/\Delta \log \sigma$) of 5·24. This value is typical of a very compressible soil. Also, as shown in Figure 12, a preconsolidation pressure of 130 kPa can be determined. This pressure corresponds to the collapse of the larger pores, which start destroying the initial microstructure of the soil.

At higher stresses, fewer pores remain intact, and the slope of the curve in the semi-log diagram decreases. This is also in a good agreement with the behaviour of soft soils at higher stresses. The smallest void ratio reached by the model at 300 kPa is 0·1, which is very dense and not physical indeed. In soft soils, small pores are located within the aggregates, between the clay platelets (see Figure 2). Experiments show that very high stresses are necessary to affect these pores. It is likely that our mechanism is more adapted to describe the collapse of inter-aggregate pores. So the void ratio to be considered here would rather be the inter-aggregates void ratio. In Canadian-sensitive clays, PSD measurements showed that the order of magnitude of this intra-aggregate pore ratio was approximately 0·6. So, in principle, values around 0·6 should be added to the inter-aggregates void ratio of Figures 12, 16 and 17, in order to provide a complete comparison with usual experimental data. Ideally, the compression of the soil on the whole range of stress should be modelled by using a second population of intra-aggregates pores, which was not made in this preliminary study.

Figure 13 shows the deformed shape of the generated pore model compared to the undeformed one, at a loading step of 120 kPa. The decrease of the volume of the pores and their displacement towards the centre of the sample are clearly illustrated. The overall deformation of the model is reasonably isotropic, showing that the choice of the pore number is adapted, and that their random disposition does not affect significantly the macroscopic response. More compression is observed in the middle of the sides of the sample, showing that ideally the ratio between the length of the external zone and the one of the internal zone containing the pores should be minimized. There is however a limit, below which numerical problems occur.

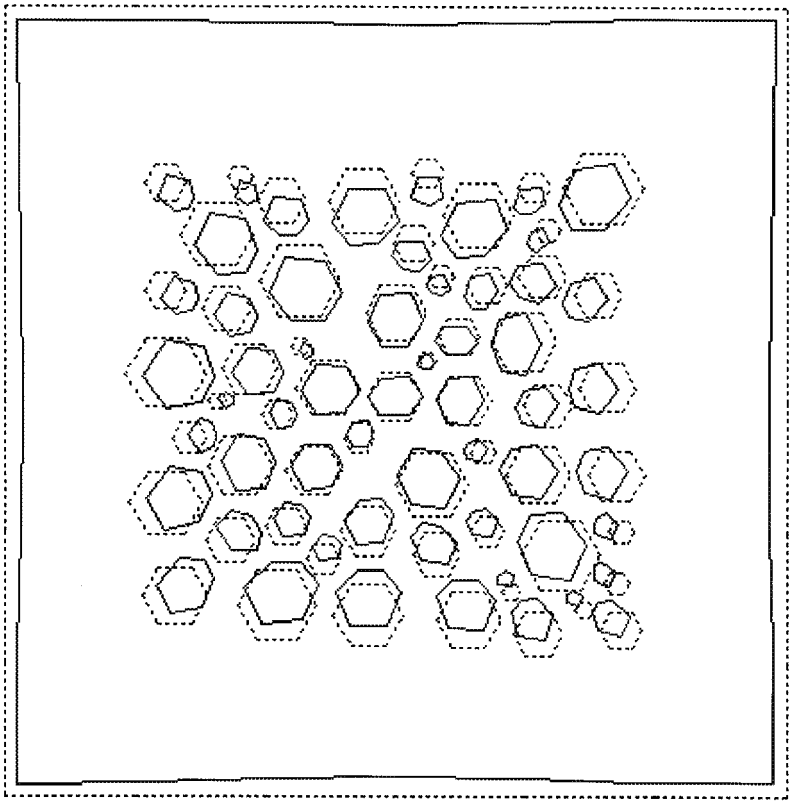

Figure 13. Deformed shape of generated pore model at 120 kPa

Figure 14 displays the evolution of the geometry of the model, according to the load increments. These figures show that the size of the pores is not the only criterion governing their collapse. Their is a marked effect of the position of the pores versus the place where the stress is applied, and pores located at the exterior of the model are destroyed before the others, even if they have a smaller radius. This is most apparent between 120 and 160 kPa.

4.2. Effect of the standard deviation of the pore distribution

It has been experimentally shown in sensitive clays that the nature of the pore distribution affected the compressibility of the sample: a well-sorted distribution corresponded to a more compressible soil (see Reference 12). Figure 15 shows the present model with a standard deviation S_{dev} equal to 0·1 μm, and the same number of pores than before (Figure 9, 58 pores). The isotropic compression curve of the sample is compared to the former one ($S_{dev} = 0{\cdot}2$ μm) in Figure 16, showing that the compressibility is increased, and confirming experimental observation. The maximum volume change is observed at the 160–180 kPa increment, with a compression index of 6·34, higher than the previous one.

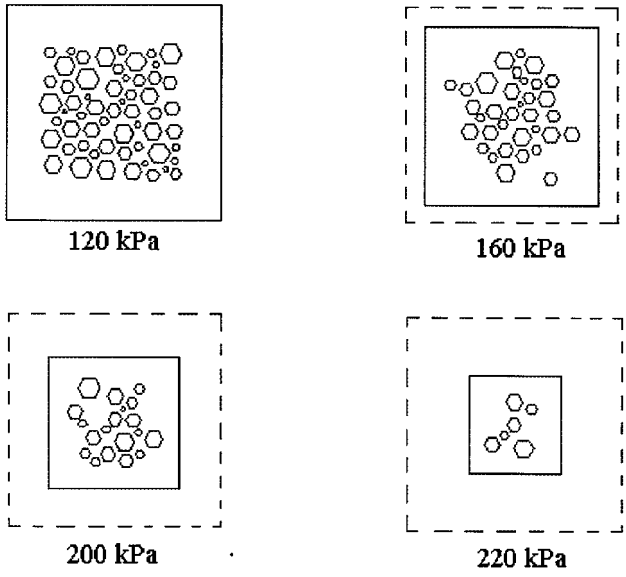

Figure 14. Different geometric configurations of the model at different steps, depending on the load level

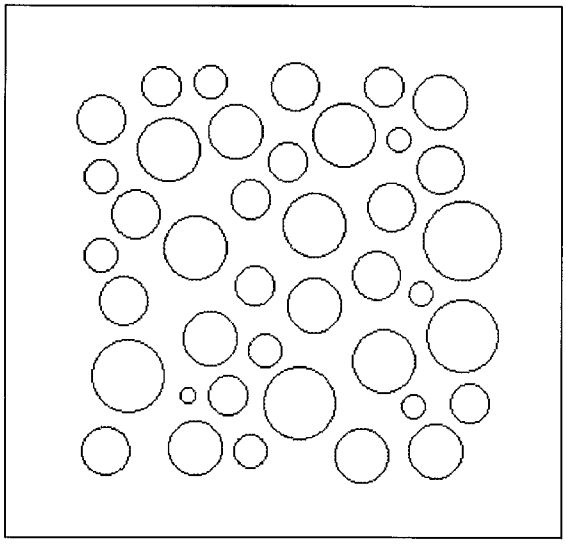

Figure 15. Distribution of pores for $S_{dev} = 0{\cdot}1$ μm

The structure effect is fairly apparent at low stresses, with no strain occurring below 120 kPa, resulting in an increase of the preconsolidation pressure. This is related to a smaller number of large pores, due to the lower value of the standard deviation. To summarize, a more sorted population of pores induces a more brittle behaviour, in good agreement with experimental results.

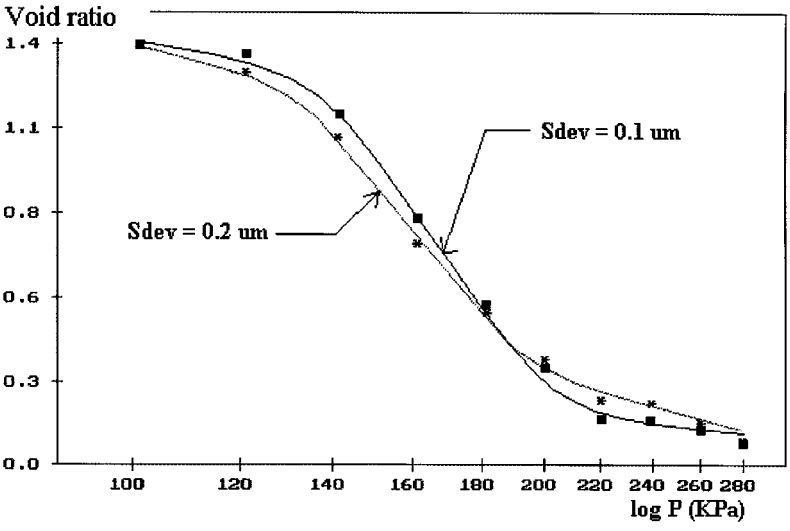

Figure 16. Comparison of the evolution of void ratio (e) VS $\log(\sigma)$ for isotropic loading process. Two Gaussian distributions: $S_{dev} = 0{\cdot}1$, $0{\cdot}2$ μm

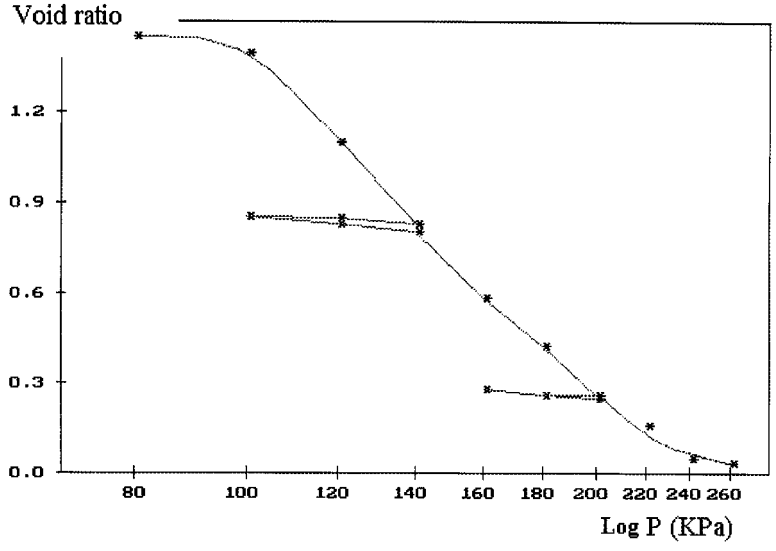

Figure 17. Evolution of void ratio (e) VS $\log(\sigma)$ for isotropic loading–unloading process

4.2. Loading–unloading process

The model depicted is Figures 9 and 10 is now subjected to a loading-unloading process in order to validate the model behaviour in unloading situations. Figure 17 shows the response of the model in a semi-log graph. Once again, the loading curve here is fairly linear in the standard

semi-logarithmic oedometric diagram. The response during the unloading–loading processes is fairly reversible at the two stress levels. The slopes, which define the C_s swelling index of the soil, are similar at the two stress levels, and not far from the initial slope at low stress, before the initiation of a significant compression. Values of 0·25 and 0·243 are obtained from Figure 17 for C_s. The C_s/C_c ratio between the swelling and compressibility indices is equal to 15, which is also satisfactory. The C_s slope is related to the compressibility of the porous matrix with no pore collapse. It can be compared to the slope above 240 kPa, where all pores have been collapsed, and where the response is provided by the solid matrix with no more pore inside. Thus, Figure 17 shows that the hardening elastoplastic volume change behaviour of soils is fairly well modelled.

5. CONCLUDING REMARKS

Most often, relationships between the microstructure of soils and their macroscopic mechanical behaviour are derived from studying the equilibrium of an assembly of grains in contact together, considering the elementary forces existing at the contacts. In this work, a different model was considered for soft clays in order to take into account the effects of the microstructure on the compressibility. The approach is derived from observations of the microstructure made by using mercury intrusion porosimetry and scanning electron microscope, on intact and compressed samples. The soil is modelled as a bidimensional porous medium made up of a linear elastic matrix containing circular pores of various sizes. The matrix obeys a Tresca failure criterion.

The calculations were carried out by using a boundary element model, which was able to contain a number of pores which keep the CPU times within reasonable limits on a standard PC. Typically, the average CPU time was of 150 min on a 486DX computer. Details of the implementation of the algorithm, as well as of the global procedure were presented. The pores of the soil are generated in a random manner, according to a previously specified Gaussian normal distribution compatible with experimental observation. When the model is subjected to an increased isotropic stress, the Tresca criterion is reached at the boundary of some pores, which collapse, resulting in a volume decrease. A remeshing procedure is then invoked in order to adjust the new microstructure. The boundary element discretization employed here has proven to be able to reproduce the complex elastic relations that exist inside the assembly of pores.

The algorithm proposed herein is also able to simulate both elastic and plastic behaviours, by simply taking into consideration the failure (collapse) of the pores as the external pressure increases. It appears from the analysis of the examples presented that the model is robust and it also allows the modelling of loading–unloading process.

The responses of the model during an isotropic compression tests are in a fairly good agreement with the volume change behaviour of fine-grained soils. The linear shape of the compression curve is a standard semi-logarithmic oedometric diagram is well reproduced, as well as the loading–unloading curves. This shows that hardening elastoplastic behaviour can be obtained at a macroscopic level by a microscopic model made of an elastic matrix with a Tresca failure criterion. The irreversible features are obtained by a mechanism of pore collapse. Experimental observations relating the compressibility of the soil to the pore size distribution curve have also been reproduced.

Some further extensions and improvements to the proposed model appear to be straightforward as, for instance, the possibility of simulating the microstructure of porous media by using a full three-dimensional boundary element model, thus allowing the analysis of some specific 3D characteristics of the soil behaviour. The extension to the analysis of partially saturated soils is

also being undertaken, as well as the possibility to apply the damage mechanics theory (see Reference 41) to evaluate the soil stresses and deformation.

ACKNOWLEDGEMENTS

The first author wishes to express his thanks to the CERMES and the Ecole Nationale des Ponts et Chaussées for the support provided for his research stay in Paris. Also, the grant given by the Consejo de Desarrollo Científico y Humanístico (Caracas) is greatly appreciated.

REFERENCES

1. P. Morlier, 'Comportement mécanique des solides poreux. Domaine élastique des corps poreux. Rôle de la pression de pore', *Rev. Industrie Minérale*, 1–17 (1970) (in French).
2. A. Casagrande, 'The structure of clay and its importance in foundation engineering. Contributions to Soil Mechanics', *J. Boston Soc. Civil Eng.*, **15,** 72–112 (1932).
3. T. W. Lambe, 'The structure of compacted clay', *ASCE J. Soil Mech. Found. Div.*, **84** (SM2), 1–34 (1958).
4. J. E. Gillott, 'Fabric of Leda clay investigated by optical, electron-optical, and X-ray diffraction methods', *Eng. Geology*, **4**(2), 133–153 (1970).
5. K. Collins and A. McGown, 'The form and function of microfabric features in a variety of natural soils', *Géotechnique*, **24,** 233–254 (1997).
6. *Proc. Int. Symp. on Soil Structure*, Gothenburg, Sweden, 1973.
7. *Proc. 4th Int. Working-Meeting on Soil Micromorphology*, Kingston, Ont., Rutherford Ed., 1973.
8. H. R. Bennett, W. R. Bryant and M. H. Hullbert, *Microstructure of Fine Grained Sediments. From Mud to Shale*, Springer, Berlin, 1991, 582p.
9. L. G. A. Aylmore and J. P. Quirk, 'Domain or turbostratic structure of clays', *Nature*, **187,** 1046–1056 (1960).
10. H. W. Olsen, 'Hydraulic flow through saturated clays', *Clays Clay Min.*, **9**(2), 131–161 (1962).
11. P. Delage and G. Lefebvre, 'Study of the structure of a sensitive Champlain clay and of its evolution during consolidation', *Canadian Geotech. J.*, **21**(1), 21–35 (1984).
12. P. Delage, 'Microstructure and compressibility of some eastern canadian sensitive soft clays', *Int. Symp. on Geotech. Eng. of Soft Soils*, Mexico, 1987, pp. 33–38.
13. P. Delage and J. P. Le. Bihan 'Microstructure et compressibilité d'argiles molles sensibles de l'Est canadien', *C.R. Acad. Sci. Paris*, 303, **II**(19), 1697–1702 (1986) (in French).
14. B. J. Botter, 'Pore collapse measurements on chalk cores', *Proc. Chalk Research Symp.*, Stavanger, Norway, 1985.
15. I. Ruddy *et al.*, 'Rock compressibility, compaction and subsidence in a high porosity chalk reservoir: a case study of Valhall field', *J. Petroleum Technol.*, **12,** 741–746 (1989).
16. Ch. Schroeder, 'Le "pore collapse": aspect particulier de l'interaction fluide-squelette dans les craies?' *C.R. Coll. Int. Groupement Belged e Mécanique des Roches*, Bruxelles, Belgium, 1995 (in French).
17. S. Leroueil and P. Vaughan, 'The general and congruent effects of structure in natural soils and weak rocks', *Géotechnique*, **40**(3), 467–488 (1990).
18. J. Goodier, 'Concentrations of stress around spherical and cylindrical inclusions and flaws', *Trans. Amer. Soc. Mech. Eng.*, **55,** 39–44 (1933).
19. J. Dominguez, 'Boundary element approach for dynamic poroelastic problems', *Int. J. Numer. Methods Eng.*, **35,** 307–324 (1992).
20. R. K. Rajapakse and T. Senjunctichai, 'An indirect boundary integral equation method for poroelasticity', *Int. j. numer. analyt. methods geomech.*, **19**(9), 587–614 (1995).
21. T. Ohkami, Y. Ichikawa and T. Kawamoto, 'A boundary element method for identifying orthotropic material parameters', *Int. j. numer. analyt. methods geomech.* **15**(9), 609–626 (1991).
22. Y. J. Chiou and S. Y. Chi, 'Boundary element analysis of Biot consolidation in layered elastic soils', *Int. j. numer. analyt. methods geomech.*, **18**(6), 377–396 (1994).
23. G. F. Chopra and G. F. Dargush, 'Boundary element analysis of stresses in axisymmetric soil mass undergoing consolidation', *Int. j. numer. analyt. methods geomech.*, **19**(3), 195–218 (1995)'.
24. M. J. Martinez and D. F. McTigue, 'A boundary integral method for steady flow in unsaturated porous media', *Int. j. numer. analyt. methods geomech.*, **16**(8), 581–602 (1992).
25. A. K. Gunstensen and D. H. Rothman, 'Lattice-Boltzman studies of two-phase flow through porous media', *J. Geophys. Res.* **98,** 6431–6441 (1992).
26. W. Soll, S. Chen, K. Eggert, D. Grunau and D. Janecky, 'Application of the lattice-Boltzmman/lattice-gas technique to multi-fluid flow in porous media', in A. Peters (ed.), *Computational Methods in Water Resources X*, Kluwer Academic Publishers, Dordrecht, 1994, pp. 991–999.

27. I. Ginzsbourg and P. M. Adler, 'Boundary flow conditions analysis for the three dimensional lattice-Boltzman model', *J. Phys. II*, **4,** 191–214 (1994).
28. A. B. McBratney and C. J. Moran, 'Soil-pore structure modelling using fuzzy random pseudofractal sets', *Proc. 9th Int. Working Meeting on Solid Micromorphology*, Townsville, Australia, 1994.
29. C. I. Moran and J. M. Kirby, 'Numerical simulation of deformation of soil-pore structure, in E. E. Alonso and P. Delage (eds), *Proc. 1st Int. Conf. on Unsaturated Soils*, Vol. 2, Balkema Publ., Rotterdam, 1995, pp. 1123–1128.
30. C. A. Brebbia, J. F. Telles and L. Wrobel, *Boundary Element Techniques: Theory and Applications in Engineering*, Springer, Berlin, 1984.
31. J. C. Lachat, 'A further development of the boundary integral technique in elastostatics', *Ph.D. Thesis*, University of Southampton, UK, 1975.
32. S. L. Crouch and A. M. Starfield, *Boundary Element Methods in Solid Mechanics*, 1st edn, George Allen & Unwin Publishers, London, U.K., 1983.
33. P. K. Bannerjee and R. Butterfield, *Boundary Element Methods in Engineering Science*, McGraw-Hall, Chichester, U.K., 1981.
34. A. E. H. Love, *A Treatise on the Mathematical Theory of Elasticity*, Dover, New York, 1927.
35. M. Cerrolaza and E. Alarcón, 'The p-adaptive BIEM approach for two-dimensional elasticity, *J. Microcomput. Civil Eng.*, **4**(1), 11–20 (1989).
36. M. Cerrolaza, 'The p-adaptive boundary integral equation method', *J. Adv. Eng. Soft.*, **15**(3/4), 261–267 (1992).
37. M. Guiggiani, G. Krishnasamy, T. J. Rudolphi and F. J. Rizzo, A general algorithm for the numerical solution of hypersingular boundary integral equations', *ASME J. Appl. Mech.*, **59,** 604–614 (1992).
38. L. J. Gray, L. F. Martha and A. R. Ingraffea, 'Hypersingular integrals in boundary element fracture analysis', *Int. j. numer. methods eng.*, **29,** 1135–1158 (1990).
39. M. Cerrolaza and E. Alarcon, 'A bicubic transformation for the numerical integration of Cauchy Principal Value integrals in boundary methods', *Int. j. numer. methods Eng.*, **29,** 987–999 (1990).
40. J. Hildebrand and G. Kuhn, 'Numerical computation of hypersingular integrals and applications to the boundary integral equation for the stress tensor', *J. Eng. Anal. Boundary Elements*, **10,** 209–217 (1992).
41. J. Lemaitre and J. L. Chaboche, *Mécanique des matèriaux solides*, Dunod, Paris, 1988 (in French).

